Development of a reinforced porcine elastin composite vascular scaffold

Monica T. Hinds,[1] Rebecca C. Rowe,[2] Zhen Ren,[2] Jeffrey Teach,[2] Ping-Cheng Wu,[2] Sean J. Kirkpatrick,[1] Kathryn D. Breneman,[2] Kenton W. Gregory,[2] David W. Courtman[3]

[1]Department of Biomedical Engineering, Oregon Health and Science University, Portland, Oregon 97006
[2]Oregon Medical Laser Center, Providence St. Vincent Medical Center, Portland, Oregon 97225
[3]St. Michael's Hospital, Departments of Surgery and Laboratory Medicine, and Institute of Biomaterials and Biomedical Engineering, University of Toronto, Toronto M5B 1W8, Canada

Abstract: Elastin, a principal structural component of native arteries, has distinct biological and mechanical advantages when used as a biomaterial; however, its low ultimate tensile strength has limited its use as an arterial conduit. We have developed a scaffold, consisting of a purified elastin tubular conduit strengthened with fibrin bonded layers of acellular small intestinal submucosa (aSIS) for potential use as a small diameter vascular graft. The addition of aSIS increased the ultimate tensile strength of the elastin conduits nine-fold. Burst pressures for the elastin composite vascular scaffold (1396 ± 309 mmHg) were significantly higher than pure elastin conduits (162 ± 36 mmHg) and comparable to native saphenous veins. The average suture pullout strength of the elastin composite vascular scaffolds was 14.612 ± 3.677 N, significantly higher than the pure elastin conduit (0.402 ± 0.098 N), but comparable to native porcine carotid arteries (13.994 ± 4.344 N). Cyclic circumferential strain testing indicated that the composite scaffolds were capable of withstanding physiological loading conditions for at least 83 h. Implantation of the elastin composites as carotid interposition grafts in swine demonstrated its superiority to clinically acceptable ePTFE with significantly longer average patency times of 5.23 h compared to 4.15 h. We have developed a biologically based elastin scaffold with suitable mechanical properties and low thrombogenicity for *in vivo* implantation, and with the potential for cellular repopulation and host integration reestablishing an appropriate elastic artery. © 2006 Wiley Periodicals, Inc. J Biomed Mater Res 77A: 458–469, 2006

Key words: elastin; scaffold; vascular grafts

INTRODUCTION

Material-related thrombosis and long-term biocompatibility remain significant limitations to currently available vascular graft materials. The most widely used and clinically successful bypass grafts are autografts, either veins or arteries, yet limited availability, due to previous use or preexisting disease, has stimulated the development of off-the-shelf alternatives that can match their performance. Bioprosthetic grafts have been under development for more than 50 years and some of these products have achieved limited clinical success. The two most successful grafts have been the ficin–digested, negatively charged, glutaraldehyde-tanned (NCGT) bovine carotid graft originally developed by Sawyer and the glutaraldehyde-tanned human umbilical vein graft originally developed by Dardik. In clinical trials, both of these grafts have demonstrated high patency rates in the treatment of peripheral vascular disease,[1,2] yet the widespread use of these devices has been markedly limited by their increased tendency for *in vivo* degeneration and aneurysm formation.[1,3] Such clinical results have lead many to speculate that bioprostheses convey a specific advantage in terms of thrombogenicity and if the problem of degenerative aneurysmal formation could be solved, these grafts may become a very promising clinical alternative. Of interest is that both the NCGT and umbilical vein grafts are substantially depleted of elastin as compared with native arteries. In fact, the original goal of ficin digestion was to remove both cells and elastin from bovine carotid arteries, leaving a tube principally composed of insol-

uble collagen.[4] Thus, bioprosthetic grafts composed principally of elastin or with an elastin content equivalent to native arteries have not as yet been developed and it is possible that elastin-rich grafts may be more resistant to aneurysmal dilatation.

Elastin, a 67-kDa extracellular matrix protein, is a major structural component of elastic arteries and is organized into a complex three-dimensional structure principally consisting of concentric layers of interconnected fenestrated fibrous sheets, the hallmark of the distinct arterial lamellar structure.[5,6] Mechanically, elastin is the principal component responsible for energy storage and recovery, and contributes to the unique dynamic tensile mechanical properties of arteries.[7] Pathologic loss of elastin has been associated with end stage aneurysm disease in older adults[8–11] and deficiency in elastin expression associated with supravalvular aortic stenosis in children.[12–15] Experiments in knock out and haploinsufficient mice have demonstrated elastin to be a very potent regulator of smooth muscle cell (SMC) phenotype and blood pressure.[16–22] As a biomaterial, elastin has several favorable properties; it is relatively resistant to degradation, can be readily purified, and preliminary studies have shown elastin-based materials to have a very low thrombogenic potential.[23,24]

A major limitation of elastin as a vascular graft material is its low ultimate tensile strength; thus, porcine small intestinal submucosa (SIS) was chosen to provide mechanical support. SIS, a collagen-based extracellular matrix scaffold, is a well established biomaterial,[25] which is currently commercially available (Cook Biotech, West Lafayette, IN) for many applications, such as hernia repair, urethral treatment, and wound care. The mechanical properties of SIS are well-matched to vascular applications, given that SIS bilayer tubular constructs have burst pressures that are comparable to those of native arteries and compliance just below that of native carotid arteries and an order of magnitude greater than synthetic grafts.[26] SIS alone as a vascular graft has shown some promising results, but requires rigorous anticoagulation therapy to prevent thrombosis and to establish an endothelial cell layer.[27–29] Although SIS appears to be ideally suited to provide an outer layer of support for vascular applications, a previous attempt to use SIS as an outer support for tissue-engineered blood vessels resulted in aneurysm formation after 6 months, hypothesized to be due to the minimal elastin fiber content.[30]

Biologically based vascular grafts have encountered clinical problems, while biological scaffolds, capable of supporting the growth of vascular cells and ultimately integrating with the host tissue, represent an attractive alternative to currently available synthetic materials. Recently, a number of scaffolds have been developed for use in tissue-engineered blood vessels, including collagen-based gels,[31–36] which lack sufficient mechanical strength, and animal sourced collagen-rich matrices,[25,26,28,37,38] which have limitations due to low endothelialization rates and high thrombogenicity. The approach chosen here was to develop an elastin-based vascular scaffold capable of becoming integrated with the host tissue after implantation, which requires low initial thrombogenicity and sufficient structural integrity to support hemodynamic loading until complete integration has occurred. To accomplish these goals, we have developed materials based on purified elastin strengthened with aSIS.

MATERIALS AND METHODS

Composite vascular scaffold

Preparation of elastin and SIS

Porcine carotid arteries were obtained from domestic swine of ~250 lb and 6–9 months of age (Animal Technologies, Tyler, TX) to size match the diameters for the acute interposition graft study. The arteries were shipped overnight in phosphate-buffered saline (PBS) on ice. The gross fat was dissected away and, using aseptic techniques, the arteries were placed in 80% ethanol for a minimum of 72 h at 4°C and subsequently treated with 0.25M NaOH for 70 min with sonication at 60°C, followed by two 30-min, 4°C washes in 0.05M HEPES (pH 7.4). The extracted elastin tubular conduits were then autoclaved at 121°C for 15 min and stored at 4°C in 0.05M HEPES.

The submucosa was isolated by physical debridment, as described by Badylak et al.,[25] from the small intestines of ~450 lb domestic swine, aged 2–5 years (Animal Technologies). The SIS was then cut into 2-in. longitudinal segments, rinsed in 0.05M HEPES, treated for 90 min with 0.1M NaOH, rinsed in 0.05M HEPES, and stored in 10% neomycin sulfate. Prior to use, the tissue segments were rinsed with 0.05M HEPES, cut longitudinally, and opened to make a sheet. These acellular SIS sheets (aSIS) were then frozen to −80°C and freeze-dried (FreeZone 6, Labconco, Kansas City, MO).

Composite scaffold construction

Fibrin was used to bond the aSIS and elastin biomaterials. Initial experiments were performed to optimize fibrinogen concentration. Lyophilized bovine fibrinogen (Sigma, St. Louis, MO) was reconstituted with 0.1M tris buffer, pH 7.4, containing 0.09% NaCl to final concentrations of 30 and 56 mg/mL. The outer surface of the elastin and the inner surface of the aSIS biomaterial were covered with the fibrinogen solution and incubated for 5 min at room temperature. Bovine thrombin (10 U/mL, Jones Pharma, St. Louis, MO) reconstituted in 0.1M tris buffer, pH 7.4, containing 0.09%
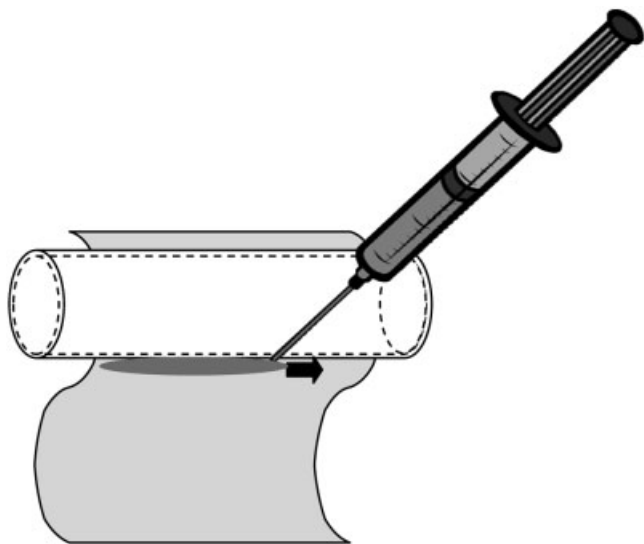
Figure 1. Schematic of the manufacturing process of the elastin composite vascular scaffold. After the outer surface of the elastin and the inner surface of the aSIS are soaked in fibrinogen, thrombin is delivered via a syringe to the aSIS, as it is wrapped around the elastin.

NaCl and 5 mM CaCl$_2$ was added to a portion of the aSIS surface, which was then wrapped onto the elastin tubular conduit; additional thrombin was added to the aSIS surface as the wrapping progressed (Fig. 1). The aSIS was wrapped twice around the elastin conduit with an additional 20% overlap. The elastin composite vascular scaffold was placed in a 37°C, 75% humidity environment overnight. The composite scaffolds were then rehydrated in 0.05M HEPES.

Histology, immunohistochemistry, and electron microscopy

The structure of the elastin composite vascular scaffold was analyzed using histology and electron microscopy methods. Paraffin-embedded sections (5-μm thick) were stained with hematoxylin & eosin and Movat's Pentachrome to evaluate the consistency of the scaffold layers. Fibrin penetration into the elastin conduits was confirmed by immunostaining with a Fibrin II monoclonal primary antibody (Accurate Chemical & Scientific, Westbury, NY). The tissue was pretreated in a steamer for 20 min, using 1 mM EDTA for antigen retrieval. The sections were run on an automated IHC stainer (Ventana Medical Systems, Tucson, AZ), incubated with the primary antibody at a dilution of 1:400 for 30 min, and then processed using the standard DAB kit (Ventana Medical Systems). Tissue samples for scanning electron microscopy were fixed with 2.5% glutaraldehyde, freeze-dried (Freezone 6, LabConco), sputter-coated (Hummer II, Technics Inc., Alexandria, VA), and viewed with a DSM 960 scanning electron microscope with LaB$_6$ source (Zeiss, Oberkochen, Germany).

In vitro testing

Tensile testing

Uniaxial tensile testing was performed on longitudinal sections of elastin tubular conduits and elastin composite vascular scaffolds, constructed with 30 mg/mL fibrinogen ($n = 6$). Dog bone shaped samples were cut to a gauge length of 20–40 mm and width of 4–6 mm with the thicknesses of the samples between 0.40 and 0.55 mm. The test samples, hydrated with 0.05M HEPES, were preconditioned at (10 ± 5)% strain at a rate of 2 Hz and then ramped to failure at a rate of 5 mm/s (500 N load cell, Tytron Micromechanical Testing System, MTS, Eden Prairie, MN). Time, displacement, and force measurements from the MTS, as well as the sample dimensions, as measured by digital calipers, were input into a custom Matlab program to determine the engineering stress–strain curves. The ultimate tensile strength, maximum failure strain, and tangent modulus at 30% strain based on a fourth-order polynomial fit were determined.

Burst, cyclic circumferential strain, and peel testing

Burst pressure testing was performed on both the elastin tubular conduits and the elastin composite vascular scaffolds ($n = 3–10$). The ends of the scaffolds were fixed in position under zero longitudinal load and then saline was infused at a rate of 100 mL/min. The pressure and diameter were continuously monitored by an inline pressure transducer (Transpac IV Monitoring kit, Abbott Labs, Chicago, IL) and a video dimension analyzer (VDA 303, Vista Electronics, Ramona, CA) both input into a Macintosh Powerbook G4 running a data acquisition program developed with Labview software.

Cyclic circumferential strain testing was performed using a vascular graft fatigue testing platform (9130–8 SGT, EnduraTEC, Minnetonka, MN). The composite vascular scaffolds were tested in a saline bath maintained at 37°C, internally pressurized with saline, and cycled at 1 Hz between 120 and 80 mmHg ($n = 5$). The outer diameter was continuously recorded with a laser micrometer and the tests were run for a minimum of 300,000 cycles or 83 h.

Peel testing was performed by manufacturing the elastin composite vascular scaffold with the final portion of aSIS left as a free flap for gripping ($n = 8$). Peel strength was determined by loading a 16-mm long scaffold on a mandrel and pulling the free flap at a 90° angle at a rate of 1 mm/s (Vitrodyne V1000, Chatillon, Greensboro, NC). The peel strength (Newton/millimeter) was calculated from the average force (Newton) divided by the specimen width (millimeter).

Suture pullout strength

Composite vascular scaffolds, elastin tubular conduits, and native porcine carotid arteries were tested for their

ability to retain sutures ($n = 5$). Test samples were anastomosed in an end-to-end fashion using a running suture of 6–0 Prolene mounted on a BV-1, 3/8 circle needle (Ethicon, Somerville, NJ). The anastamosis was centrally located between the two pneumatic side action grips (Instron, Canton, MA) with a total specimen length between the grips of 22 ± 3 mm. Tissue was maintained in a hydrated state at room temperature and tested to failure at a displacement rate of 5 mm/s (858 Mini Bionix II, MTS). Failure force was determined from the peak of the force–displacement curve. Each specimen was observed until failure, with the failure mechanism recorded.

Acute porcine interposition graft study

Aseptic processing was used to manufacture six composite scaffolds for implantation into a swine model. In these scaffolds, the thrombin within the fibrin layers was inhibited by pretreatment with 0.15 μg of PPACK (Calbiochem, San Diego, CA) to block residual active thrombin. Spectrozyme TH Assays (American Diagnostica, Stamford, CT) confirmed that this concentration was sufficient for the amount of thrombin used (data not shown).

National Institutes of Health (NIH) guidelines for the care and use of laboratory animals (NIH Publication No. 85–23 Rev. 1985) were observed for all animal experiments. Bilateral carotid interposition grafts were implanted in a total of six domestic swine of ~220 lb, aged 6–9 months. Animals were sedated with Telazol 4–9 mg/kg, i.m., and anesthesia was maintained with Isoflurane. Normal saline was delivered intravenously at a rate of 200 cm³/h. A femoral cutdown was performed and a 6–7Fr sheath placed to monitor blood pressure and to catheterize for angiography. O_2 saturation, blood pressure, temperature, activated clotting time (ACT), and heart rate were recorded every 30 min during the procedure.

Carotid arteries were exposed and treated with Papaverine:Lidocaine (1:4) solution to locally dilate the vessels. Intravenous heparin (100 U/kg) was given before cross-clamping the arteries and the ACT was maintained above 250 s during the graft implantation period. Doppler flow probes (Transonic Systems, Ithaca, NY) were placed distal to the anastomotic site and coupled to the artery using ultrasound jelly. The exposed carotid artery was cross-clamped, divided in the center, and 1 cm resected. The stumps of the artery were flushed with heparin, the grafts were implanted in an end-to-end fashion using a running suture of 6–0 Prolene, and after completing the anastomoses, the proximal and distal clamps were released, respectively. This procedure was repeated for the ePTFE control graft (4 mm diameter, GORE-TEX®, W.L. Gore & Associates, Flagstaff, AZ) on the contralateral artery.

Angiography of both carotid arteries was performed after implantation and at study endpoint. At study endpoint, saline was infused into the carotids, the arteries were clamped and the grafts were explanted and rinsed.

Experimental design

In each animal, the elastin composite vascular scaffold (average diameter of 4.3 ± 0.3 mm and length of 4.0 ± 0.6 cm) was implanted first into either the left or right common carotid, determined randomly, and an equal length ePTFE control graft (GORE-TEX®, 4 mm diameter) was then implanted on the contralateral side. The ePTFE graft was chosen as a control due to the clinical acceptance of this material for vascular grafts, and both the lack of suture strength and low burst pressures of the pure elastin scaffolds. The study was continued for 6 h or until both of the grafts occluded as determined by the Doppler flowrate readings at which point both grafts were excised. The excised grafts were opened longitudinally, photographed, and examined grossly for evidence of thrombi. Grafts were then cross-sectioned at 5-mm intervals. Alternate sections were snap frozen for cryoembedding, fixed in 10% neutral-buffered formalin for paraffin embedding, or fixed in 2.5% glutaraldehyde for SEM analysis. Tissue was processed for histological staining or electron microscopy as described earlier to evaluate thrombosis on the surface and cell infiltration into the elastin composite vascular scaffold.

RESULTS

Composite vascular scaffold

We have successfully constructed over 200 composite vascular scaffolds from porcine derived arterial elastin, fibrin glue, and sheets of aSIS (Fig. 2). The composites displayed handling characteristics similar to native arteries [Fig. 2(A)]. Histological examination more clearly revealed the unique composite structure of the scaffold [Fig. 2(B)]; the outer (adventitial) portion of the composite is composed of two layers of the predominantly collagenous aSIS bonded together with a distinct band of fibrin with a second band of fibrin bonding the aSIS to the purified lamellar elastin structure comprising the media. Bonding between layers is likely enhanced by a deep penetration of the fibrin into both the elastin and aSIS [Fig. 2(C)].

SEM of the internal composite scaffold surface showed an intact elastin fibrillar structure typical of native porcine carotid arteries (Fig. 3). The elastin fiber diameters were 0.5–3 μm with the predominant orientation in the longitudinal direction. In some regions, the fibrillar structure appears to fuse into a fenestrated sheet, and in these regions, fenestrations in the internal elastic lamellar unit range in size from 2–5 μm in these unstrained samples.

In vitro testing

Tensile testing

The stress–strain curve of the vascular scaffold contained profiles typical of a collagen and elastin
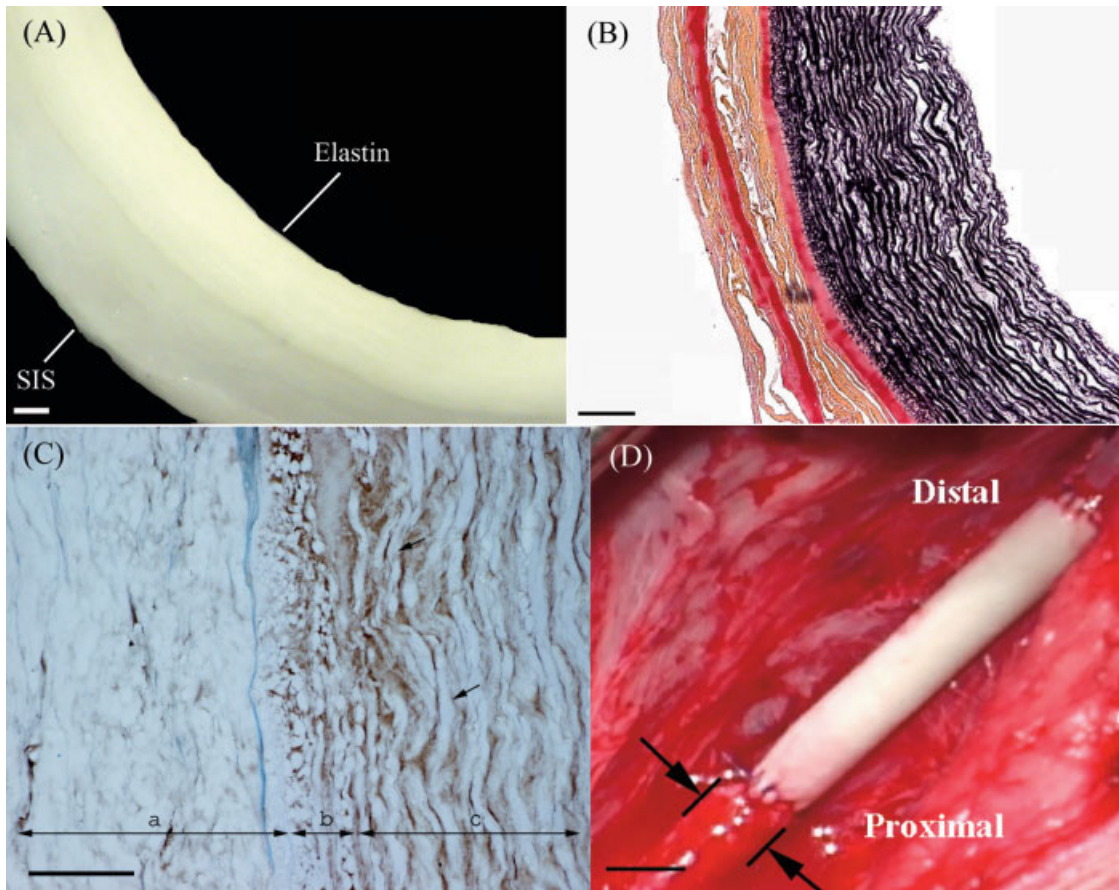
Figure 2. (A) The elastin composite vascular scaffold was constructed with an inner surface of pure porcine elastin and an outer aSIS, bound together by fibrin. The bar indicates 100 μm. (B) Representative histology image of the elastin composite vascular scaffold (Movat's Pentachrome stain, bar represents 100 μm). The lamellar structure of the pure elastin (black) comprised a significant portion of the thickness of the elastin composite vascular scaffold. Good apposition of the layers was attained with the fibrin adhesive (red). (C) Fibrin II staining (brown) of the elastin composite scaffold. Region (a) indicates the aSIS region, region (b), the transitional region and in region (c), single arrows point to the elastin lamellae. The bar represents 10 μm. (D) Gross image of elastin composite vascular scaffold as a carotid interposition graft. The bar indicates 6 mm.

composite material (Fig. 4). The composite failed in three distinct phases with the initial failure point supporting the highest loading. We have interpreted the failure as the initial delamination of the aSIS layers, followed by breakage of individual aSIS layers, and finally low load failure of the elastin. This interpretation is supported by the observed mode of failure and the failure modes of the individual components, with the high collagen content in the aSIS supporting the highest loads and the final section typical of the more linear high strain failure of elastin.[39] The results displayed an order of magnitude increase in both UTS ($p < 0.001$, t test) and tangent modulus ($p < 0.02$, t test) of the composite material over that of purified elastin (Table I). Published data on the ePTFE indicated an order of magnitude increase in both UTS and Modulus compared with the elastin composite vascular scaffold.[40]

Burst, cyclic circumferential strain, and peel testing

Burst pressure testing was performed on elastin tubular conduits, cut to 2.54 cm length with an average initial diameter of 5.53 ± 0.54 mm, and three formulations of the elastin composite vascular scaffolds, including (A) 30 mg/mL fibrinogen with fully hydrated aSIS (3.64 ± 0.75 cm length and 6.87 ± 0.40 mm initial outer diameter), (B) 30 mg/mL fibrinogen with freeze dried aSIS (3.33 ± 0.35 cm length, 7.06 ± 1.29 mm initial outer diameter), and (C) 56 mg/mL fibrinogen with freeze dried aSIS (2.39 ± 0.71 cm length, 6.50 ± 0.27 mm initial outer diameter). The conduits composed of elastin alone had an average burst pressure of 162 ± 36 mmHg ($n = 10$), while composite scaffold formulations had higher burst pressures of (A) 349 ± 53 mmHg ($n = 3$), (B) 894 ± 222 mmHg ($n = 3$), and (C) 1396 ± 309 mmHg ($n = 9$) (Fig. 5 and Table I). The burst pressure of formulation (C)
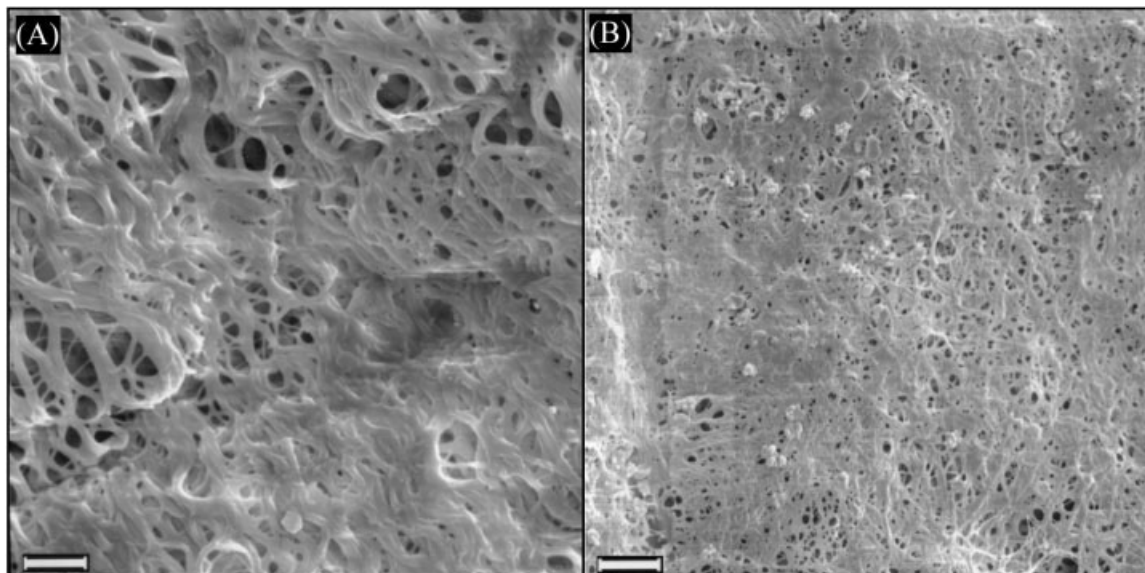
Figure 3. Scanning electron microscopy images of the lumen of the elastin composite vascular scaffold indicated that the lamellar structure of native arteries is maintained in this matrix. (A) This image, taken prior to implantation, indicates that the elastin fibers are 0.5–3 μm in diameter and the predominant axis of orientation is longitudinal. The scale bar indicates 10 μm. (B) In the patent vessels, there was evidence of isolated platelet adhesion. The scale bar indicates 20 μm.

was significantly higher than both the elastin alone and formulation (B) ($p < 0.001$, ANOVA, Tamhane post hoc). Therefore, formulation (C) was used for all further testing.

The cyclic circumferential strain test parameters were chosen to evaluate the scaffolds for gross delamination of the elastin and SIS layers under pulsatile conditions. All composite scaffolds held pressure, without leaks, for the entire test period of at least 83 h. The peel testing determined that the average peel

Figure 4. A typical stress–strain curve of the dog bone shaped specimen of the elastin composite vascular scaffold, which was preconditioned and pulled to failure. The materials failed first by delamination of the layers, followed by breakage of the aSIS layers, and subsequent elastin failure.

strength of the composite scaffold was 0.019 ± 0.005 N/mm ($n = 8$) (Table I).

Suture testing

The addition of the fibrin-aSIS layers to the elastin biomaterial significantly increased the suture failure load (Fig. 6). When sutured to native porcine carotid arteries, pure elastin tubular conduits failed at the suture line. In marked contrast, the reinforced elastin composite vascular scaffolds did not fail, rather the native arteries were the point of failure. The composite vascular scaffold sutured to native arteries had an average suture failure load of 14.612 ± 3.677 N, nearly 40-fold higher than that of the elastin biomaterial (0.402 ± 0.098 N, $p < 0.001$, ANOVA, Bonferroni post hoc). The suture failure load of the composite vascular scaffold-to-native artery samples was no different than the native-to-native artery, nor the composite-to-composite samples (ANOVA, NS).
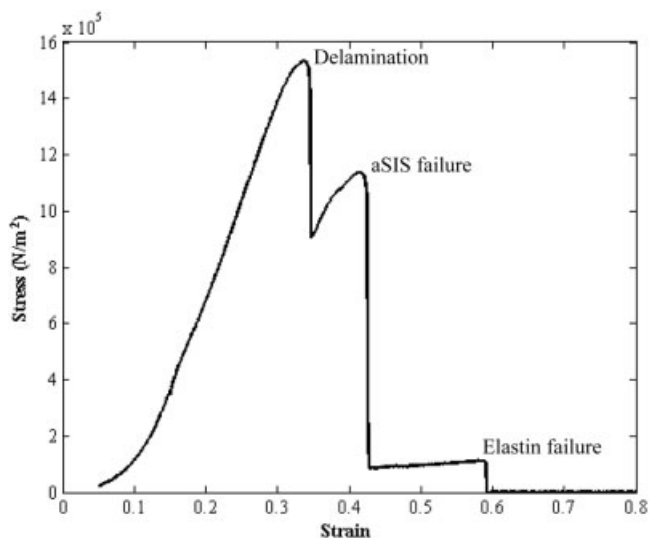
Animal study

All six elastin composite vascular scaffolds were successfully sutured as interpositional grafts in the carotid artery of domestic swine with no significant difference in crossclamp times compared with the ePTFE controls (32 ± 12 min vs. 25 ± 7 min, $p = 0.17$, Paired t test). Gross images [Fig. 2(D)] and angiography indicated minimal size mismatch with the native

Comparison of Mechanical Properties of Elastin Composite Vascular Scaffold to Elastin Conduit

Test	Elastin Composite Vascular Scaffold	Elastin Conduit	ePTFE Control[a]
Ultimate tensile strength (MPa)	1.744 ± 0.278*	0.196 ± 0.067	14.1 ± 1.3
Max strain	0.453 ± 0.172	0.571 ± 0.100	0.477 ± 0.105
Tangent modulus at 30% strain (MPa)	6.578 ± 3.181*	0.268 ± 0.056	55.2 ± 5.2
Burst pressure (mmHg)	1396 ± 309*	162 ± 36	
Peel strength (N/mm)	0.019 ± 0.005	N/A	
Cyclic (h)	≥83	N/A	

*$p < 0.02$, compared to purified elastin conduit.
[a] ePTFE data from ringed segments of 23 um internodal distance ePTFE at a 0.4%/s strain rate.[40]

artery. The implanted composite scaffolds displayed physiological pulses similar to the native artery as noted through visual observations.

The domestic swine implantation model used represents an aggressive thrombosis challenge; heparin is only administered during implantation, resulting in a transient increase of ACT times, which return to baseline ACT levels within 90 min (Fig. 7). The elastin composite vascular scaffold always performed equal to or better than the ePTFE control graft during the 6-h implant study. Not only did the composite vascular scaffold have a better patency rate of 33% (2/6) compared to 16.5% (1/6), the average patency times were significantly longer for the composite vascular scaffolds, 5:14 ± 1:00, compared with 4:09 ± 1:01 for the ePTFE control grafts (Fig. 8, $p < 0.05$, Paired t test).

The average patency times were determined by the Doppler flow measurements (and confirmed with angiography) with 6 h used for the fully patent vessels.

The gross images (Fig. 9) demonstrate the range of reactions to the elastin composite scaffold. Two of the six vessels had clean surfaces with no thrombus formation [Fig. 9(A)], while the remaining four scaffolds had isolated thrombi [Fig. 9(B)], which is most likely an injury response related to the suture line, rather than a reaction to the material. When clotted, the ePTFE control grafts contained pervasive thrombi [Fig. 9(C)]. Histology sections indicated cell infiltration of varying degrees into the elastin composite scaffold, while the ePTFE grafts were typically filled with red blood cells and minimal mononuclear cells [Fig. 9(D–G)]. Some immunohistochemical staining on
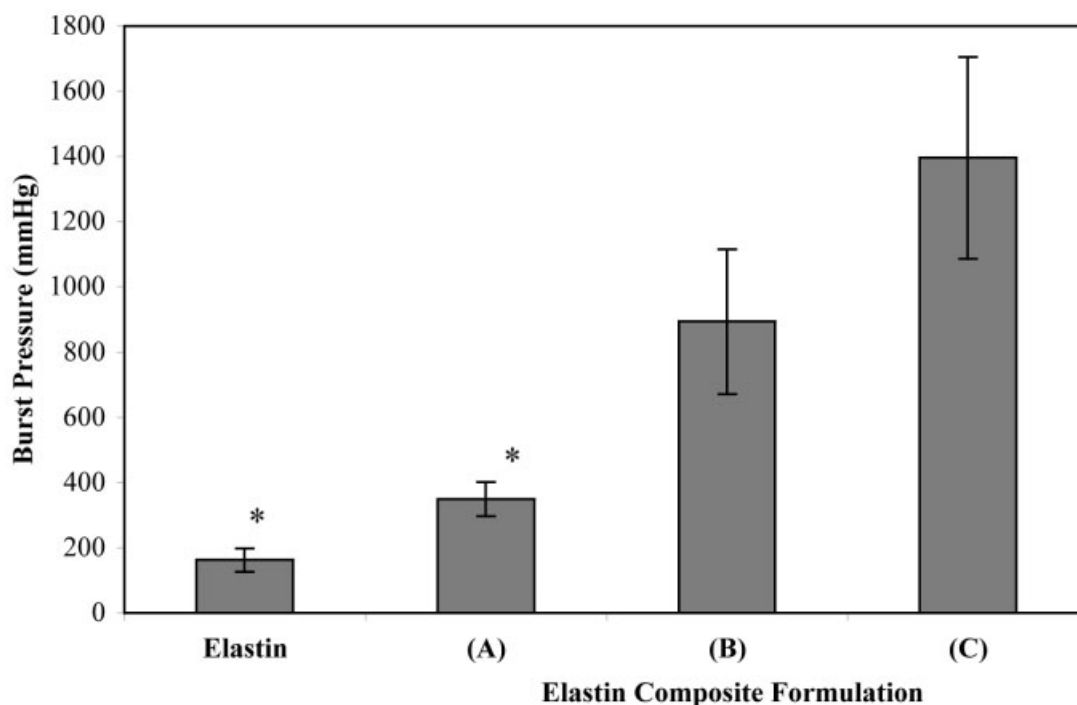

Figure 5. Average burst pressures of the pure elastin conduits and three formulations of the elastin composite vascular scaffold (average ± standard deviation). Increasing the concentration of fibrinogen and lyophilizing the aSIS prior to attachment increased the burst strength. Formulation (C) had significantly higher burst pressures than elastin alone or composite formulation (A) (*$p < 0.001$, ANOVA, Tamhane post hoc).
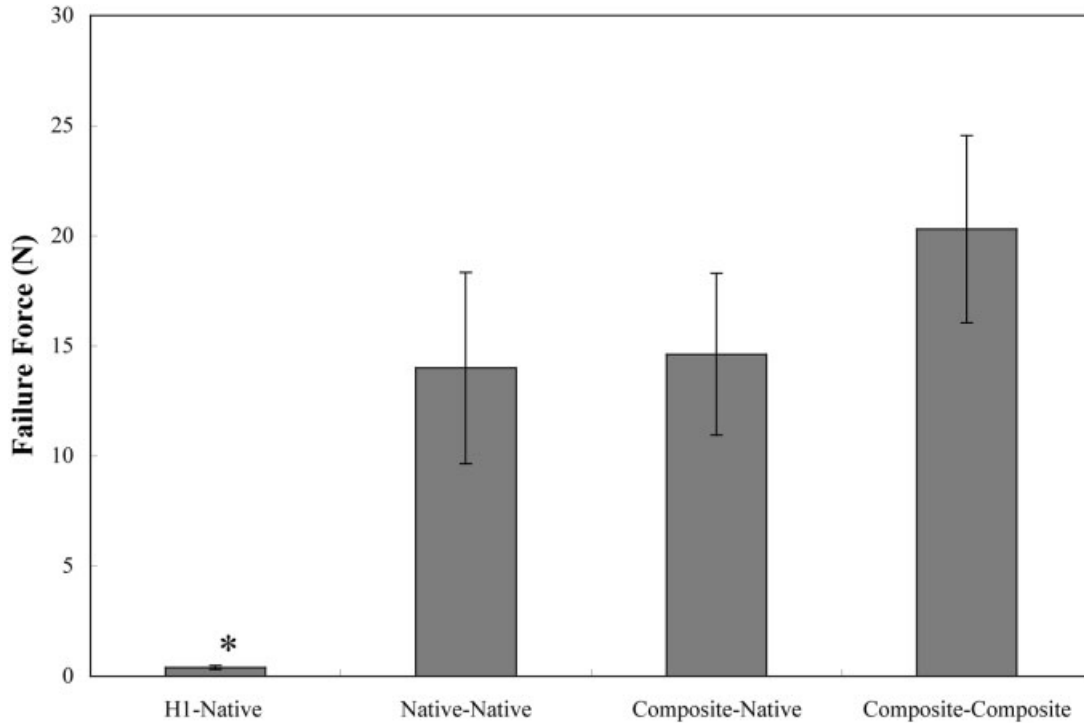
Figure 6. Average suture failure forces of native arteries sutured to pure elastin conduits, native arteries, and elastin composite vascular scaffolds, as well as composite scaffolds sutured to composite scaffolds (average ± standard deviation). The suture strength of the elastin conduits, where the elastin fractured first, was significantly lower than the three other specimens (*$p < 0.001$, ANOVA, Bonferroni post hoc). The failure point of the native-native and native-composite samples always occurred on the native artery.
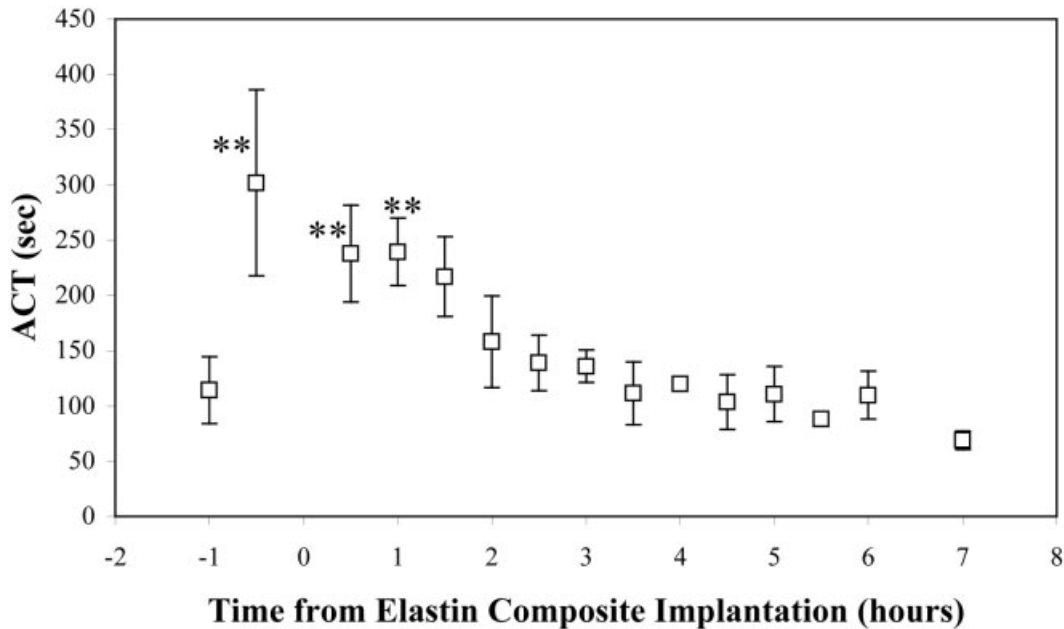

Figure 7. Average active clotting times (ACTs) as measured throughout the acute implantation. ACTs were taken prior to implantation (-60 min) and within an average of 30 ± 11 min prior to elastin composite scaffold implantation (-30 min) and every 30 min throughout the procedure (average ± standard deviation). The times of the readings were normalized to the implantation time of the elastin composite scaffold and grouped in 30-min intervals. Only the -30, 30, and 60 min time points were significantly different from the preimplant values, indicating that within 90 min of the composite scaffold implantation, the heparin has been rapidly metabolized by the swine (**$p < 0.01$, ANOVA, Bonferroni).
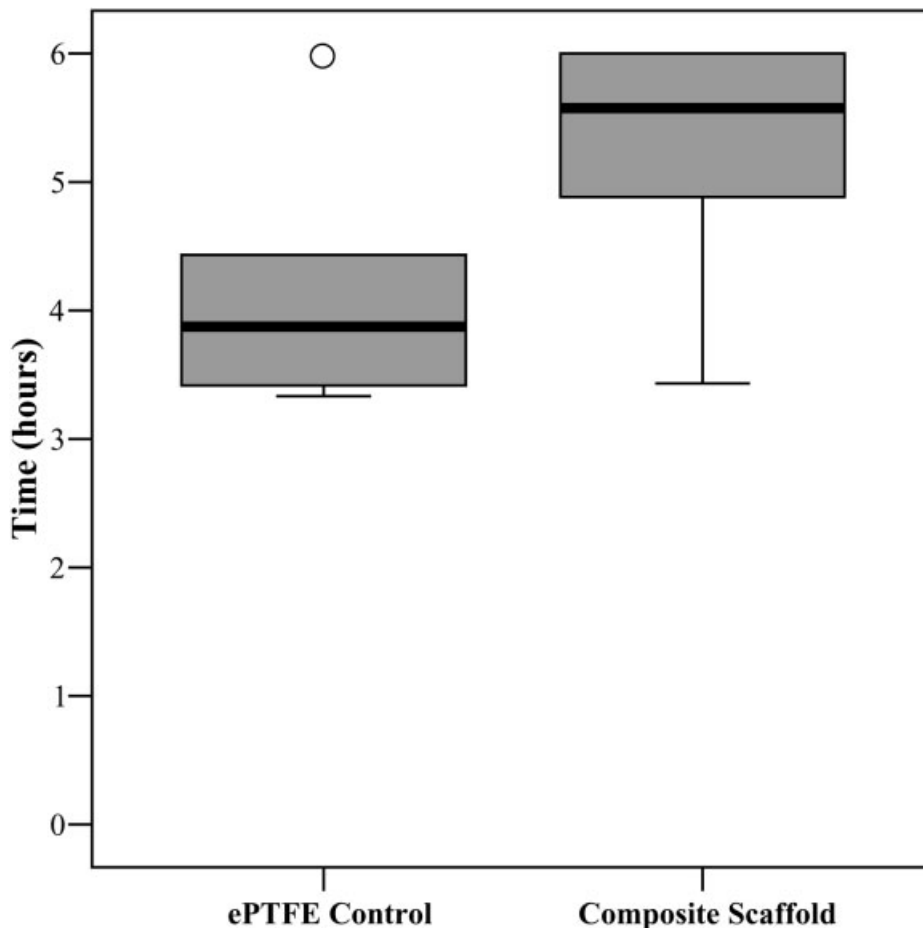
Figure 8. Box plot of occlusion times indicating the median, quartiles, and extreme values, with 6 h assigned to the patent vessels (average ± standard deviation). In all cases the occlusion times were equivalent or longer for the elastin composite vascular scaffold compared to the ePTFE control graft. The average time to occlusion for the composite vascular scaffold was significantly longer than the ePTFE graft (***$p < 0.05$, Paired t-test). A single outlier is designated by the circle.

elastin composite scaffold sections indicated that a small percentage of the infiltrated cells are of mono-cyte/macrophage lineage, while the remaining nucleated cells are lymphocytes or polymorphs.

DISCUSSION

The elastic fiber is an important structural element of the arterial wall that not only plays a fundamental role in elastic energy recovery but is also a regulator of cell phenotype. As a biomaterial, elastin has many favorable characteristics such as a resistance to degradation and a low thrombogenic potential. However, use of pure elastin conduits has been limited by its low ultimate tensile strength and the difficulty of reconstituting an appropriate fiber structure. We describe here, for the first time, a method of manufacturing a purified tubular elastin conduit reinforced with wraps of small intestinal submucosa adhered to the adventitial surface with polymerized fibrin. We have opti-

mized the hydration and fibrinogen concentrations to maximize the burst pressures of the conduit, producing a nine-fold increase over purified elastin alone. Burst and ultimate tensile strength values of our composite scaffold are comparable to that of native vessels.[37,41] In these optimized composite vascular scaffolds, suture pull-out strength was equivalent to that of a native vessel. Acute thrombogenicity studies demonstrated that the elastin composite vascular scaffolds perform statistically better than clinically available 4-mm ePTFE vascular grafts. Our goal was to construct a biological scaffold principally consisting of elastin, but reinforced to withstand arterial pressures over acute implantation periods; such a scaffold can also be used in tissue engineering experiments as a substrate for vascular cell repopulation.

Currently available synthetic vascular bypass grafts display adequate performance in the peripheral vascular circulation, yet autologous vein, when available, remains the graft of choice.[42] Although synthetic grafts are more readily available and easily implant-
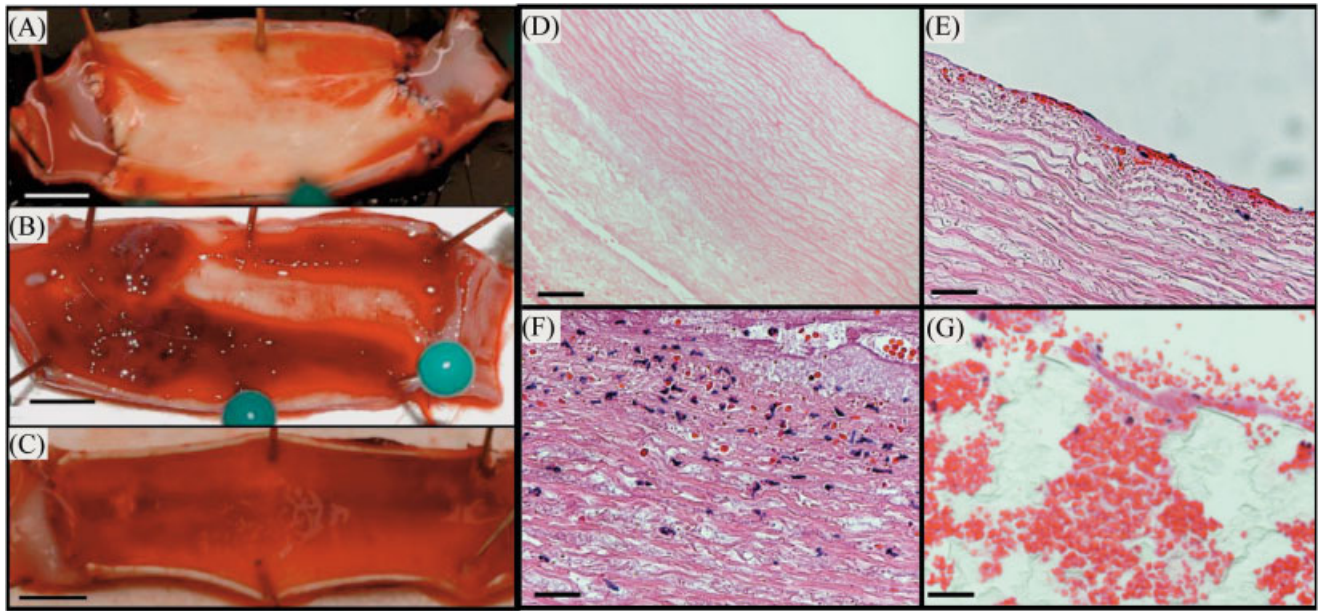
Figure 9. Gross images of explanted grafts with (A) patent elastin composite vascular scaffold and (B) and (C) occluded specimen of elastin composite vascular scaffold and ePTFE control graft, respectively from the same animal. The thrombus in the elastin composite vascular scaffold appears to be associated with the suture line, while it is throughout the ePTFE control graft. Scale bars indicate 0.5 cm. (D–G) Histological images of the explanted grafts stained with Hematoxylin and Eosin. Cell infiltration into the elastin composite vascular scaffold varied from minimal cells in (D) and (E–F) maximal penetration depths of 130 μm. The animal with minimal cell infiltration into the elastin composite vascular scaffold (D) and (E) had an ePTFE control graft filled with red blood cells throughout artery wall. Scale bars indicate (D) 100 and 25 μm in (E–G).

able, it is widely believed that autologous veins display enhanced patency over the long term.[43] Indeed, biological grafts in general display a high freedom from thrombotic failure, yet often fail by pathologic remodeling leading to aneurysm formation or extensive intimal hyperplasia (an arterialization response in vein grafts).[44,45] The therapeutic potential of biological grafts have driven an extensive research effort directed towards the correction of these aberrant remodeling responses. Recent studies suggest that molecular approaches may indeed prove to be beneficial in limiting vein graft hyperplasia.[46,47] However, such cellular modifications will not correct a key defect in current biological grafts, that is, the absence of an appropriate arterial extracellular matrix. Development of biological materials containing an elastic fiber structure more representative of that in the arterial wall may be essential, as depletion or loss of elastin has been correlated to both aneurysmal progression and severe SMC hyperplasia in both animals and humans.[8–11,18–21] It has been proposed that a key defect in tissue-engineered arteries is the lack of a mature elastic tissue structure.[30] The work presented in this study represents an initial attempt in the development of a vascular scaffold based on a purified arterial elastic fiber structure, and such a scaffold will allow us to better define the role of the elastic fiber in longer term implant remodeling.

Using a purified elastin conduit as the basis of our vascular scaffold, allowed us to reconstitute a complete arterial elastin matrix in which both the elastin content and fiber structure of a natural artery are restored. The ability of this elastin-based scaffold to store and return energy to the circulation was at least partially replicated in our vascular scaffold, as evidenced by visual pulsation similar to that of a native artery both after implantation and during cyclic circumferential strain testing. The utility of elastin as an arterial flow surface has been demonstrated in elastin-covered stents implanted in a porcine coronary model, which demonstrated high patency with significantly reduced intimal hyperplasia in elastin-covered stents compared with uncovered stents.[19] Our porcine graft implantation animal model represents a robust thrombotic challenge with greater than 80% of clinically available ePTFE grafts occluding within 6 h. This is likely due to the extensive arterial injury (arterial bisection and anastamosis) and the use of a single heparin dose, leading to a rapid return of ACTs to baseline levels within 90 min of implantation. Thus, this model was designed not as a predictor of long term patency under optimal anticoagulant therapy but rather as a direct test of acute thrombogenicity. In our model, there was no instance where the elastin occluded first, and in five of the six animals, it failed after the ePTFE control graft with one occurring at the same time. Thus, the elastin conduits displayed a sig-

nificant increase in acute patency, suggesting that the flow surface is superior to clinically available ePTFE.

In constructing the elastin composite scaffold, fibrin was chosen to adhere the aSIS layers to the purified elastin conduit. Fibrin is a naturally occurring polymer and as such is non-toxic, biocompatible, and resorbable, and fibrin sealants have been successfully used in many surgical applications.[48] The structure of the fibrin gel, its strength, rate, and extent of polymerization can be regulated by temperature and the concentration of fibrinogen, thrombin, Factor XIII, or calcium.[49–51] Numerous studies have demonstrated a correlation between adhesive shear strength and fibrinogen concentration.[52–54] Commercially available fibrin sealants have a range of fibrinogen concentrations of 50–100 mg/ml and thrombin concentrations of 216–1247 U/ml.[55] Our optimal fibrin formulation contains similar fibrinogen levels (56 mg/ml), but is polymerized with much lower thrombin concentrations (10 U/ml), and by using low thrombin levels initially applied at room temperature, we were able to slow polymerization and produce optimal penetration into the adherent tissue structure. Unlike *in vivo* situations where rapid hemostasis may be required,[56] we determined that polymerization over a more prolonged curing period optimized the ease of manufacturing and burst pressure strengths. Although the fibrin bonding is able to produce adequate initial strength, the integrity of the scaffold over the long term will most likely depend on cellular repopulation and consequent remodeling of the collagen matrix both of which may be enhanced by the resorbable nature of the fibrin bond.

We have developed a vascular scaffold, principally composed of purified elastin, which can withstand arterial pressure, has a favorable low thrombogenic potential, and is a promising material in terms of host cell integration. As one of the first elastin-based materials capable of being implanted into the arterial circulation, this scaffold may be a useful tool in studies designed to explore *in vivo* vascular cell-matrix interactions and may in time lead to the development of relevant elastin-based biomaterials.

References

1. Sawyer PN, Fitzgerald J, Kaplitt MJ, Sanders RJ, Williams GM, Leather RP, Karmody A, Hallin RW, Taylor R, Fries CC. Ten year experience with the negatively charged glutaraldehyde-tanned vascular graft in peripheral vascular surgery. Initial Multicenter Trial. Am J Surg 1987;154:533–537.

2. Dardik H, Wengerter K, Qin F, Pangilinan A, Silvestri F, Wolodiger F, Kahn M, Sussman B, Ibrahim IM. Comparative decades of experience with glutaraldehyde-tanned human umbilical cord vein graft for lower limb revascularization: An analysis of 1275 cases. J Vasc Surg 2002;35:64–71.

3. Strobel R, Boontje AH, Van Den Dungen JJ. Aneurysm formation in modified human umbilical vein grafts. Eur J Vasc Endovasc Surg 1996;11:417–420.

4. Sawyer PN, O'Shaughnessy AM, Sophie Z. Development and performance characteristics of a new vascular graft. J Biomed Mater Res 1985;19:991–1010.

5. Clark JM, Glagov S. Transmural organization of the arterial media. The lamellar unit revisited. Arteriosclerosis 1985;5:19–34.

6. Wolinsky H, Glagov S. A lamellar unit of aortic medial structure and function in mammals. Circ Res 1967;20:99–111.

7. Roach MR, Burton AC. The reason for the shape of the distensibility curves of arteries. Can J Biochem Physiol 1957;35:681–690.

8. Baxter BT, McGee GS, Shively VP, Drummond IA, Dixit SN, Yamauchi M, Pearce WH. Elastin content, cross-links, and mRNA in normal and aneurysmal human aorta. J Vasc Surg 1992;16:192–200.

9. Gandhi RH, Irizarry E, Cantor JO, Keller S, Nackman GB, Halpern VJ, Newman KM, Tilson MD. Analysis of elastin cross-linking and the connective tissue matrix of abdominal aortic aneurysms. Surgery 1994;115:617–620.

10. Hunter GC, Dubick MA, Keen CL, Eskelson CD. Effects of hypertension on aortic antioxidant status in human abdominal aneurysmal and occlusive disease. Proc Soc Exp Biol Med 1991;196:273–279.

11. Rizzo RJ, McCarthy WJ, Dixit SN, Lilly MP, Shively VP, Flinn WR, Yao JS. Collagen types and matrix protein content in human abdominal aortic aneurysms. J Vasc Surg 1989;10:365–373.

12. Curran ME, Atkinson DL, Ewart AK, Morris CA, Leppert MF, Keating MT. The elastin gene is disrupted by a translocation associated with supravalvular aortic stenosis. Cell 1993;73:159–168.

13. Ewart AK, Jin W, Atkinson D, Morris CA, Keating MT. Supravalvular aortic stenosis associated with a deletion disrupting the elastin gene. J Clin Invest 1994;93:1071–1077.

14. Li DY, Toland AE, Boak BB, Atkinson DL, Ensing GJ, Morris CA, Keating MT. Elastin point mutations cause an obstructive vascular disease, supravalvular aortic stenosis. Hum Mol Genet 1997;6:1021–1028.

15. Urban Z, Michels VV, Thibodeau SN, Donis-Keller H, Csiszar K, Boyd CD. Supravalvular aortic stenosis: A splice site mutation within the elastin gene results in reduced expression of two aberrantly spliced transcripts. Hum Genet 1999;104:135–142.

16. Broder K, Reinhardt E, Ahern J, Lifton R, Tamborlane W, Pober B. Elevated ambulatory blood pressure in 20 subjects with Williams syndrome. Am J Med Genet 1999;83:356–360.

17. Eronen M, Peippo M, Hippala A, Raatikka M, Arvio M, Johansson R, Kahkonen M. Cardiovascular manifestations in 75 patients with Williams syndrome. J Med Genet 2002;39:554–558.

18. Faury G, Pezet M, Knutsen RH, Boyle WA, Heximer SP, McLean SE, Minkes RK, Blumer KJ, Kovacs A, Kelly DP, Li DY, Starcher B, Mecham RP. Developmental adaptation of the mouse cardiovascular system to elastin haploinsufficiency. J Clin Invest 2003;112:1419–1428.

19. Karnik SK, Brooke BS, Bayes-Genis A, Sorensen L, Wythe JD, Schwartz RS, Keating MT, Li DY. A critical role for elastin signaling in vascular morphogenesis and disease. Development 2003;130:411–423.

20. Li DY, Brooke B, Davis EC, Mecham RP, Sorensen LK, Boak BB, Eichwald E, Keating MT. Elastin is an essential determinant of arterial morphogenesis. Nature 1998;393:276–280.

21. Li DY, Faury G, Taylor DG, Davis EC, Boyle WA, Mecham RP, Stenzel P, Boak B, Keating MT. Novel arterial pathology in mice and humans hemizygous for elastin. J Clin Invest 1998; 102:1783–1787.

22. Rose C, Wessel A, Pankau R, Partsch CJ, Bursch J. Anomalies of the abdominal aorta in Williams-Beuren syndrome—Another cause of arterial hypertension. Eur J Pediatr 2001;160: 655–658.

23. Bordenave L, Lefebvre F, Bareille R, Rouais F, Baquey C, Rabaud M. New artificial connective matrix-like structure: Thrombogenicity and use as endothelial cell culture support. Biomaterials 1992;13:439–447.

24. Woodhouse KA, Klement P, Chen V, Gorbet MB, Keeley FW, Stahl R, Fromstein JD, Bellingham CM. Investigation of recombinant human elastin polypeptides as non-thrombogenic coatings. Biomaterials 2004;25:4543–4553.

25. Badylak SF, Lantz GC, Coffey A, Geddes LA. Small intestinal submucosa as a large diameter vascular graft in the dog. J Surg Res 1989;47:74–80.

26. Roeder R, Wolfe J, Lianakis N, Hinson T, Geddes LA, Obermiller J. Compliance, elastic modulus, and burst pressure of small-intestine submucosa (SIS), small-diameter vascular grafts. J Biomed Mater Res 1999;47:65–70.

27. Huynh T, Abraham G, Murray J, Brockbank K, Hagen PO, Sullivan S. Remodeling of an acellular collagen graft into a physiologically responsive neovessel. Nat Biotechnol 1999;17: 1083–1086.

28. Sandusky GE Jr, Badylak SF, Morff RJ, Johnson WD, Lantz G. Histologic findings after in vivo placement of small intestine submucosal vascular grafts and saphenous vein grafts in the carotid artery in dogs. Am J Pathol 1992;140:317–324.

29. Sandusky GE, Lantz GC, Badylak SF. Healing comparison of small intestine submucosa and ePTFE grafts in the canine carotid artery. J Surg Res 1995;58:415–420.

30. Opitz F, Schenke-Layland K, Cohnert TU, Starcher B, Halbhuber KJ, Martin DP, Stock UA. Tissue engineering of aortic tissue: Dire consequence of suboptimal elastic fiber synthesis in vivo. Cardiovasc Res 2004;63:719–730.

31. Furukawa KS, Ushida T, Toita K, Sakai Y, Tateishi T. Hybrid of gel-cultured smooth muscle cells with PLLA sponge as a scaffold towards blood vessel regeneration. Cell Transplant 2002; 11:475–480.

32. He H, Matsuda T. Arterial replacement with compliant hierarchic hybrid vascular graft: Biomechanical adaptation and failure. Tissue Eng 2002;8:213–224.

33. He H, Matsuda T. Newly designed compliant hierarchic hybrid vascular graft wrapped with microprocessed elastomeric film-II: Morphogenesis and compliance change upon implantation. Cell Transplant 2002;11:75–87.

34. Kanda K, Matsuda T, Oka T. In vitro reconstruction of hybrid vascular tissue. Hierarchic and oriented cell layers. ASAIO J 1993;39:M561–M565.

35. Tranquillo RT. The tissue-engineered small-diameter artery. Ann NY Acad Sci 2002;961:251–254.

36. Skalak TC, Little CD, Mcntire LV, Hirschi KK, Tranquillo RT, Post M, Ranieri J. Vascular assembly in engineered and natural tissues: Breakout session summary. Ann NY Acad Sci 2002;961: 255–257.

37. Roeder RA, Lantz GC, Geddes LA. Mechanical remodeling of small-intestine submucosa small-diameter vascular grafts—A preliminary report. Biomed Instrum Technol 2001;35:110–120.

38. Woods AM, Rodenberg EJ, Hiles MC, Pavalko FM. Improved biocompatibility of small intestinal submucosa (SIS) following conditioning by human endothelial cells. Biomaterials 2004;25: 515–525.

39. Sherebrin MH, Song SH, Roach MR. Mechanical anisotropy of purified elastin from the thoracic aorta of dog and sheep. Can J Physiol Pharmacol 1983;61:539–545.

40. Catanese J III, Cooke D, Maas C, Pruitt L. Mechanical properties of medical grade expanded polytetrafluoroethylene: The effects of internodal distance, density, and displacement rate. J Biomed Mater Res 1999;48:187–192.

41. Cohuet G, Challande P, Osborne-Pellegrin M, Arribas SM, Dominiczak A, Louis H, Laurent S, Lacolley P. Mechanical strength of the isolated carotid artery in SHR. Hypertension 2001;38:1167–1171.

42. Merrell GA, Gusberg RJ. Infrainguinal bypass conduit: Autogenous or synthetic—A national perspective. Vasc Endovasc Surg 2002;36:247–254.

43. Canver CC. Conduit options in coronary artery bypass surgery. Chest 1995;108:1150–1155.

44. Memon AQ, Huang RI, Marcus F, Xavier L, Alpert J. Saphenous vein graft aneurysm: Case report and review. Cardiol Rev 2003;11:26–34.

45. Baklanov DV, Peters KG, Seidel AL, Taylor DA, Annex BH. Neovascularization in intimal hyperplasia is associated with vein graft failure after coronary artery bypass surgery. Vasc Med 2003;8:163–167.

46. Mann MJ, Gibbons GH, Kernoff RS, Diet FP, Tsao PS, Cooke JP, Kaneda Y, Dzau VJ. Genetic engineering of vein grafts resistant to atherosclerosis. Proc Natl Acad Sci USA 1995;92:4502–4506.

47. Ehsan A, Mann MJ, Dell'Acqua G, Tamura K, Braun-Dullaeus R, Dzau VJ. Endothelial healing in vein grafts: Proliferative burst unimpaired by genetic therapy of neointimal disease. Circulation 2002;105:1686–1692.

48. Donkerwolcke M, Burny F, Muster D. Tissues and bone adhesives-historical aspects. Biomaterials 1998;19:1461–1466.

49. Galanakis DK, Lane BP, Simon SR. Albumin modulates lateral assembly of fibrin polymers: Evidence of enhanced fine fibril formation and of unique synergism with fibrinogen. Biochemistry 1987;26:2389–2400.

50. Hardy JJ, Carrell NA, McDonagh J. Calcium ion functions in fibrinogen conversion to fibrin. Ann NY Acad Sci 1983;408: 279–287.

51. Okada M, Blomback B. Factors influencing fibrin gel structure studied by flow measurement. Ann NY Acad Sci 1983;408:233–253.

52. Sierra DH, Eberhardt AW, Lemons JE. Failure characteristics of multiple-component fibrin-based adhesives. J Biomed Mater Res 2002;59:1–11.

53. Marx G, Mou X. Characterizing fibrin glue performance as modulated by heparin, aprotinin, and factor XIII. J Lab Clin Med 2002;140:152–160.

54. Glidden PF, Malaska C, Herring SW. Thromboelastograph assay for measuring the mechanical strength of fibrin sealant clots. Clin Appl Thromb Hemost 2000;6:226–233.

55. Dickneite G, Metzner H, Pfeifer T, Kroez M, Witzke G. A comparison of fibrin sealants in relation to their in vitro and in vivo properties. Thromb Res 2003;112:73–82.

56. Saltz R, Dimick A, Harris C, Grotting JC, Psillakis J, Vasconez LO. Application of autologous fibrin glue in burn wounds. J Burn Care Rehabil 1989;10:504–507.